Ion Time-of-Flight Signals from Nanosecond Laser Ablation Plasmas Excited in Constricted Cavities

J. E. Hernandez[1, a)] and M. Wada[1, b)]

[1]*Graduate School of Science and Engineering, Doshisha University, Kyotanabe, Kyoto 610-0321, Japan*

[a)]Corresponding author: cyjd3302@mail4.doshisha.ac.jp
[b)]mwada@doshisha.ac.jp

Abstract. Ion time-of-flight spectra from nanosecond pulse laser ablation at 1064 nm wavelength of a graphite target under repeated 10 Hz pulse repetition are investigated. By injecting focused laser beams at 12° from the surface normal, the ablated target formed a vertical cavity as the target is rotated continuously. For increasing number of pulses, decrease in positive signals for positive ion extraction while increase in negative signals for both 5 and 20 GW/cm^2 laser power densities at -3 kV extraction voltage were observed. Increase in voltage onto a positive ion retardation plate installed in front of the Faraday cup array showed distinct negative ion peaks with decrease in positive ion signal intensity. Time-of-flight signals under increased number of pulses with the positively biased retardation plate showed less pronounced negative ion peaks for 5 GW/cm^2 at -3 kV extraction, whereas the peaks persisted for 20 GW/cm^2 laser power density. The influence of target cavity development on the negative ion formation is discussed.

INTRODUCTION

Nanosecond laser ablation has been employed as positive and negative cluster ion sources for mass spectrometry [1-3]. The dominant mechanisms in nanosecond laser ablation involve target melting, vaporization, phase explosion, and plasma formation [4]. As the laser plasma is formed near the target surface, various many-body interactions such as collisions between ions, electrons, and neutral particles occur within the plasma, wherein collisions cool down the laser produced plasma due to kinetic energy loss leading to condensation and aggregation of the ablated particles, forming heavy positive ions [5]. These collisions also influence the formation of negative ions. It was suggested that one of the major mechanisms in the formation of negative ions within the laser plasma involves the collisions of electrons with the neutral atoms due to the high electron density within the plasma plume [6]. By increasing the collision probability, negative ion formation would be enhanced via electron attachment process. In laser plasmas, the free electrons involved in the attachment mechanism are due to thermionic emission and surface ionization [7, 8]. However, negative ions could also be destroyed via electron collision detachment processes as negative ions are neutralized by electron impact [9]. These processes emphasize the significance of factors affecting the production of these negative ions via collisional processes. One such factor is the installation of an external barrier impeding the plasma plume free expansion. Increasing the collision probability by means of laser ablation within the inner diameter of a rotating hollow cylindrical target has been showed previously in detecting negative carbon ions via time-of-flight (TOF) spectroscopy with the target as a barrier of plume propagation [10]. However, the influence of the plasma plume constriction on the negative ion formation mechanisms has not been investigated.

In this work, TOF signals of a plasma produced by a nanosecond pulsed laser incident on a rotating graphite target under repeated ablation are investigated. When the laser strikes the target surface at the same region, a hole is drilled with which the expansion of a laser plasma initiated within the hole is constricted. Ion signals are analyzed by varying the laser power density, extraction voltage, and positive ion retardation voltage, where the possible mechanisms involved in negative ion formation are discussed.

EXPERIMENTAL SETUP

A Q-switched Nd:YAG laser at 1064 nm wavelength at 10 Hz repetition rate is incident on a plano-convex lens, and is focused on the center of a 10 mm diameter cylindrical graphite target surface at a 12º angle with respect to the beam extraction axis, whose schematic is shown in Fig. 1(a). The laser is initially aligned to strike the target center in order to provide axial symmetry during repeated ablation. The laser spot size on the target is approximately 1 mm. The target is rotated with a DC motor at 18 rpm during continuous ablation at 5 GW/cm^2 laser power density.

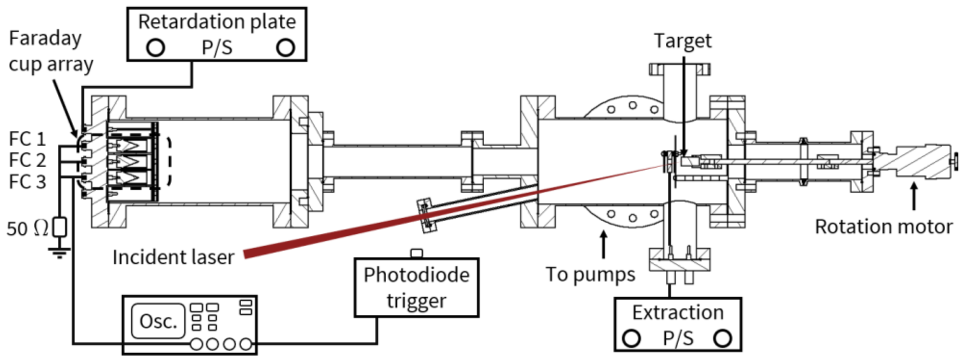

(a)

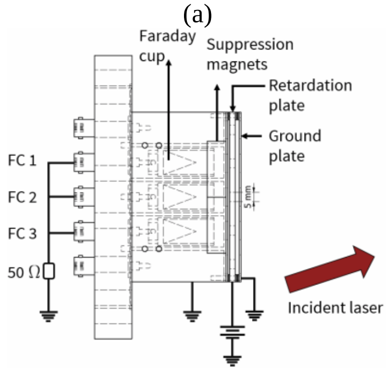

(b)

FIGURE 1. (a) Schematic of the laser ion source (b) Schematic of the Faraday cup array equipped with retarding plate

TABLE 1. Parameters of the laser ion source

Parameter	Value
Laser wavelength	1064 nm
Laser pulse width	5 ns
Target material	Graphite
Base pressure	4 x 10^{-6} Pa

In investigating the effect of laser power density on the resulting ion signals, the laser power is increased or decreased by tuning the Q-switch trigger delay from the optical pumping. In order to extract positive and negative ions, an extraction electrode consisting of a bias plate placed 9 mm from the target, which is situated between two grounded plates at 3 mm spacing with 5 mm aperture diameters. Positive or negative bias from -3 to 3 kV extraction voltage is employed to accelerate negative or positive ions, respectively.

The ions are collected via a Faraday cup (FC) array placed 60 cm from the target, whose schematic is shown in Fig. 1(b). The FC array consists of three grounded collectors FC 1, FC 2, and FC 3 enclosed in a grounded shield, each with a 9 mm aperture placed -18, 0, and 18 mm away from the target axis, where the last is situated nearest to the incident laser port. Neodymium permanent magnets are attached to the FC array with a magnetic flux density of 300 G measured 5 mm in front of the array to suppress incoming electrons. To exclude low energy positive ions from the laser plasma plume, an electrostatic ion retardation plate with 4 mm thickness and 5 mm aperture diameter is attached 2 mm in front of the Faraday cup array, whose bias is tuned up to 600 V. A 1 mm grounded plate with 9 mm aperture diameter is attached 2 mm in front of the retarding plate. The distance between the axes of each Faraday cup apertures is 18 mm. Each collector within the array is terminated with a 50 Ω resistor, where the time-of-flight (TOF) signals are measured using an oscilloscope. Signals are triggered by a high-speed photodiode synchronized with the arrival of the laser onto the carbon target. Time-of-flight signals detected were averaged for 16 pulses to increase shot-to-shot reliability. The laser ion source parameters are shown in Table 1.

RESULTS

Fresh Target Ablation

Figure 1 shows the typical TOF signal temporal distribution detected by the Faraday cup array for a fresh target. The major peak at 5 μs corresponds to C_3^+ cluster ions typically found in free expansion of laser produced carbon plasmas [11]. The Faraday cup 2 (FC 2) positioned along the beam axis is observed to acquire the highest positive signal intensity compared to the adjacent collectors. In Fig. 2(b), TOF spectra from 1-3 kV extraction voltage show increase in positive signal before the C_3^+ peak. On the other hand, the increase of negative signal before this peak is observed for -2 and -3 kV extraction.

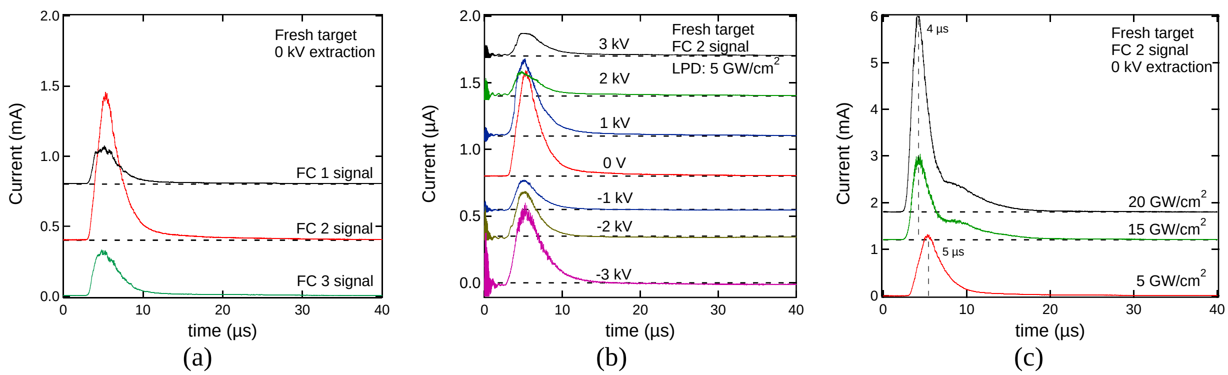

FIGURE 2. (a) Time-of-flight signal distribution for a fresh target (b) TOF signals from -3 kV to 3 kV extraction voltage (c) TOF spectrum of FC 2 for increasing laser power densities

The TOF signals for the fresh target are also investigated with increasing laser power density. In Fig. 2(c), the ion TOF spectra are shown for 5, 15, and 20 GW/cm^2 laser power densities. Positive ion yield increases with laser power density due to the additional ablated mass induced by higher laser fluence. For 15 and 20 GW/cm^2 laser power densities, broad positive ion distributions after the C_3^+ peak are observed which are attributed to heavy clusters after increased target vaporization. For these laser power densities, the positive peaks are shifted approximately 1 μs earlier due to the higher laser energies which propel the ions towards the detectors at a higher kinetic energy.

Ion Production from a Cavity Formed Target

During cavity drilling by laser ablation at 10 Hz repetition rate and 5 GW/cm^2 laser power density, the graphite target is axially rotated at 18 revolutions per minute. After the ablation run, deposits are observed around the extraction plate aperture which are due to ejected neutrals along with the formed plasma plume. Micrographs of the target before and after 30000 pulses ablation are shown in Fig. 3(a). After ablation, a rim is formed near the hole due to target evaporation during ablation. The target cross section is inspected where a narrow cavity is formed whose walls constrict the plasma initiated deep within the hole. This hole is characterized as the ablation depth whose maximum depth is measured. Shown in Fig. 3(b) is the ablation depth with increasing number of pulses, where approximately 3 mm hole depth is measured after 30000 shots. The decrease in the change of the depth as the number of pulses is increased is attributed to the increased plasma shielding formed within the cavity as the plasma plume formation is initiated deep within the hole [12]. An inspection of the hole formed on the target shows the surface damage in the vicinity of the cavity which could be due to the rapid heat transfer within the cavity walls. Since the time interval between laser shots is longer compared to the time of ion formation, each subsequent pulse is not influenced by the previous pulse.

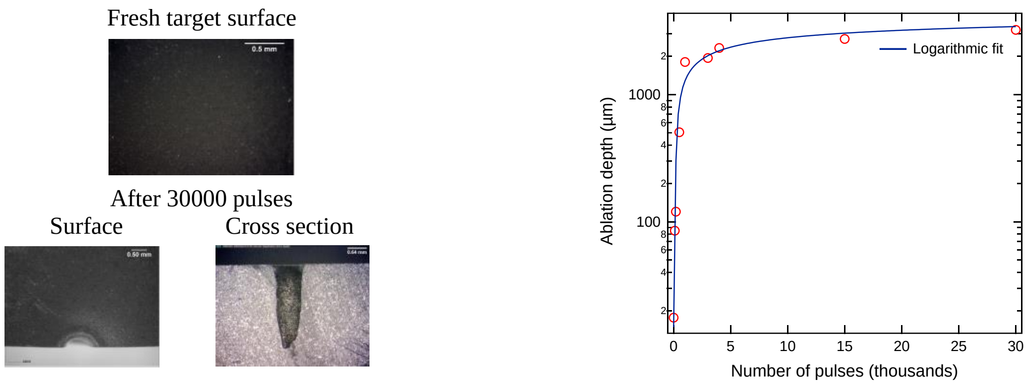

(a) (b)

FIGURE 3. (a) Micrographs of target surface and cross-section (b) Target cavity depth for increasing number of pulses

Ion spectra for increasing number of pulses without extraction voltage at 5 and 20 GW/cm^2 are shown in Fig. 4. Significant decrease of C_3^+ ion peak is observed for the first 10000 pulses for both laser power densities. Broad positive signals are observed for 20 GW/cm^2 laser power density, as shown in Fig. 4(b). The ion signals are integrated from 20 µs to 30 µs time of flight in order to visualize the signal evolution after the C_3^+ carbon ion peak, obtaining the charge yield as shown in Fig. 4(c). For 5 GW/cm^2 laser power density, the total charge decreased by approximately 70 percent relative to the initial value for the first 10000 pulses. The charge yield decrease becomes smaller for subsequent pulses, which is due to the lower difference in the amount of ablated mass as the number of shots is increased above 5000 pulses. For 20 GW/cm^2 laser power density, approximately 65 percent of charge decrease is observed for the first 5000 pulses. Subsequent pulses up to 30000 shots also show slower charge yield decrease. The charge yield of 20 GW/cm^2 laser power density is observed to be greater than that of the lower laser power density, which indicates the production of larger amount of slower positive ions after the main carbon peak.

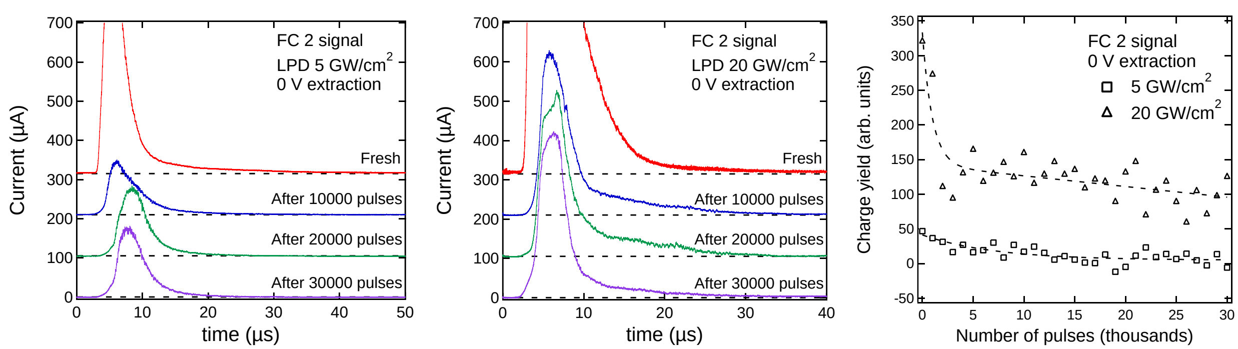

(a) (b) (c)

FIGURE 4. Ion time-of-flight spectra of FC 2 for increasing number of pulses for (a) 5 GW/cm^2 and (b) 20 GW/cm^2 laser power densities (c) Time integration of TOF current signals of (a) and (b) from 20 to 30 µs at 5 and 20 GW/cm^2 laser power densities for increasing number of laser shots; dashed lines represent exponential line fits

Ion Extraction

Time-of-flight signals obtained from accelerated positive and negative ions from the laser plasma for fresh and after 30000 pulses target condition and from -3 to 3 kV extraction potential are shown in Fig. 5. For the fresh target after 3 kV extraction voltage at 5 GW/cm^2 laser power density, fast positive signal is detected in all Faraday cups followed by the main carbon ion peak, which decreases after approximately 12 µs, shown in Fig. 5(a). As the number of pulses is increased, the positive signal decreased due to the smaller number of ions coming out the target surface as a result of increased cavity depth. A 2 μs shift in the rising edge of the main carbon peak towards later times is also observed for both 3 kV and -3 kV extraction voltages at 5 GW/cm^2 laser power density. At -3 kV extraction voltage, negative signals are detected for all Faraday cups before 5 μs. These negative signals may represent fast negative ions since the electron Larmor radius corresponds to 0.1 mm for a 1 μs time-of-flight and 300 G magnetic field in front of the FC array. Increase in negative signals after the main positive carbon peak is observed for both laser power densities at -3 kV extraction voltage, which also corresponds to a negative ion distribution.

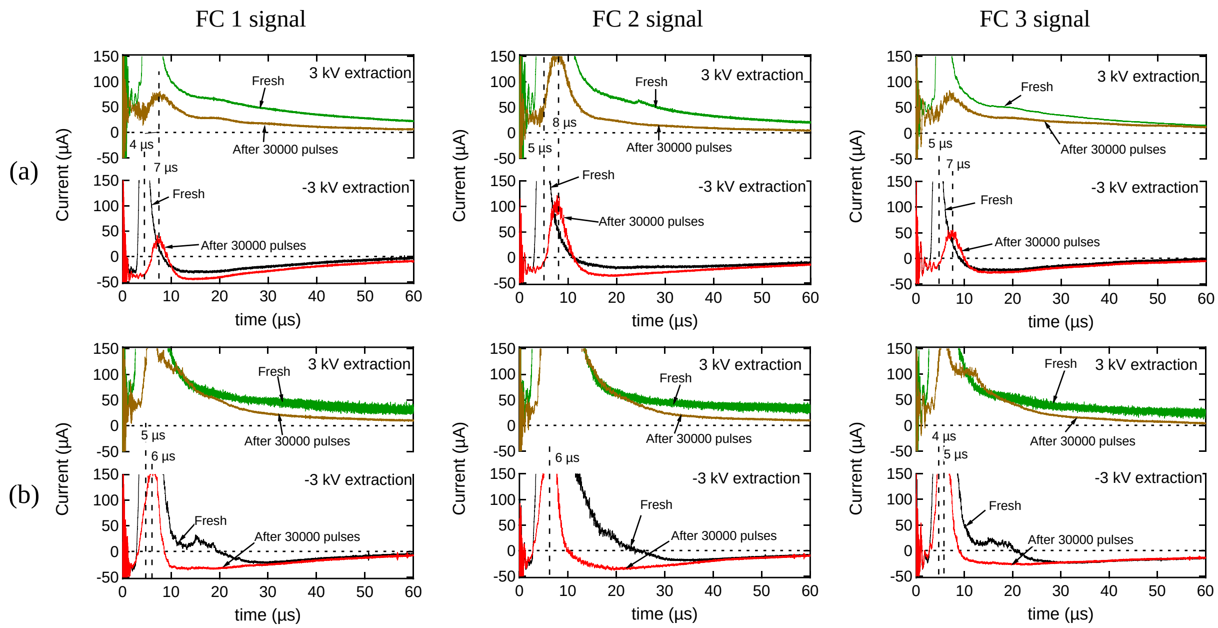

FIGURE 5. Faraday cup signal distributions for 3 and -3 kV extraction potential for fresh and ablated target after 30000 pulses for (a) 5 and (b) 20 GW/cm^2 laser power densities

In order to further analyze these negative signals after the main carbon peak, experiments are performed for negative ion extraction by suppressing the extracted positive ions using the Faraday cup array equipped with an electrostatic potential ion retardation plate, shown in Fig. 1 (b). Figure 6 shows the time-of-flight signals under fresh ablation at -3 kV extraction voltage with varying retardation plate voltages. Trace negative signals are detected for increasing retardation plate voltages, which represent negative ion peaks arriving towards the detector, compared with the spectrum at 0 V bias which showed a broad negative signal TOF distribution. At 5 GW/cm^2 laser power density, broad peak distributions are observed from 25 to 28 μs TOF from 500 V to 600 V front plate bias, as shown in Fig. 6(a). At this laser power density, the onset at which the negative peaks start to appear occurs above 100 V bias. This suggests that the repelled positive ions from the laser plasma has a threshold energy at this potential. Figure 6(b) shows the time-of-flight signals for 20 GW/cm^2 laser power density wherein the amount of detected positive and negative signals increased compared to that of the lower laser power density. Negative ion peaks start to appear from 100 V plate bias at 20 GW/cm^2, which is lower than the case with 5 GW/cm^2 laser power density where peaks start to emerge above 200 V. This could be due to the higher laser power which allows for the increased number of ablated particles contributing to collisions which form negative ions. Increase of the retardation plate voltage revealed distinct peaks ranging from 29 to 33 μs with a sharp peak at 31 μs at 600 V retardation potential, which corresponds to masses of approximately 1440 amu. Figure 6(c) shows the signals after 30000 pulses for varying retardation plate bias at 5 GW/cm^2 laser power density at -3 kV extraction voltage. As the deep cavity is formed, the positive peaks at 5 μs significantly decreased for all retardation plate voltages, with no distinct detection of negative ion peak. The main peak for 20 GW/cm^2 laser power density at -3 kV extraction voltage also significantly decreased while double positive ion peaks at 2.8 and 5 μs from 400 to 600 V retardation plate voltage are observed at this extraction voltage, as shown in Fig. 6(d). Moreover, distinct negative peaks are still detected from 100 V retardation plate bias at 20 GW/cm^2 laser power density. This indicates that the positive and negative ions gain energy due to the higher power density laser which are ejected from the cavity muzzle. Broad negative peak distributions from 400 to 600 V retardation potential are detected from 25 to 32 μs with the highest negative ion peak at 27 μs.

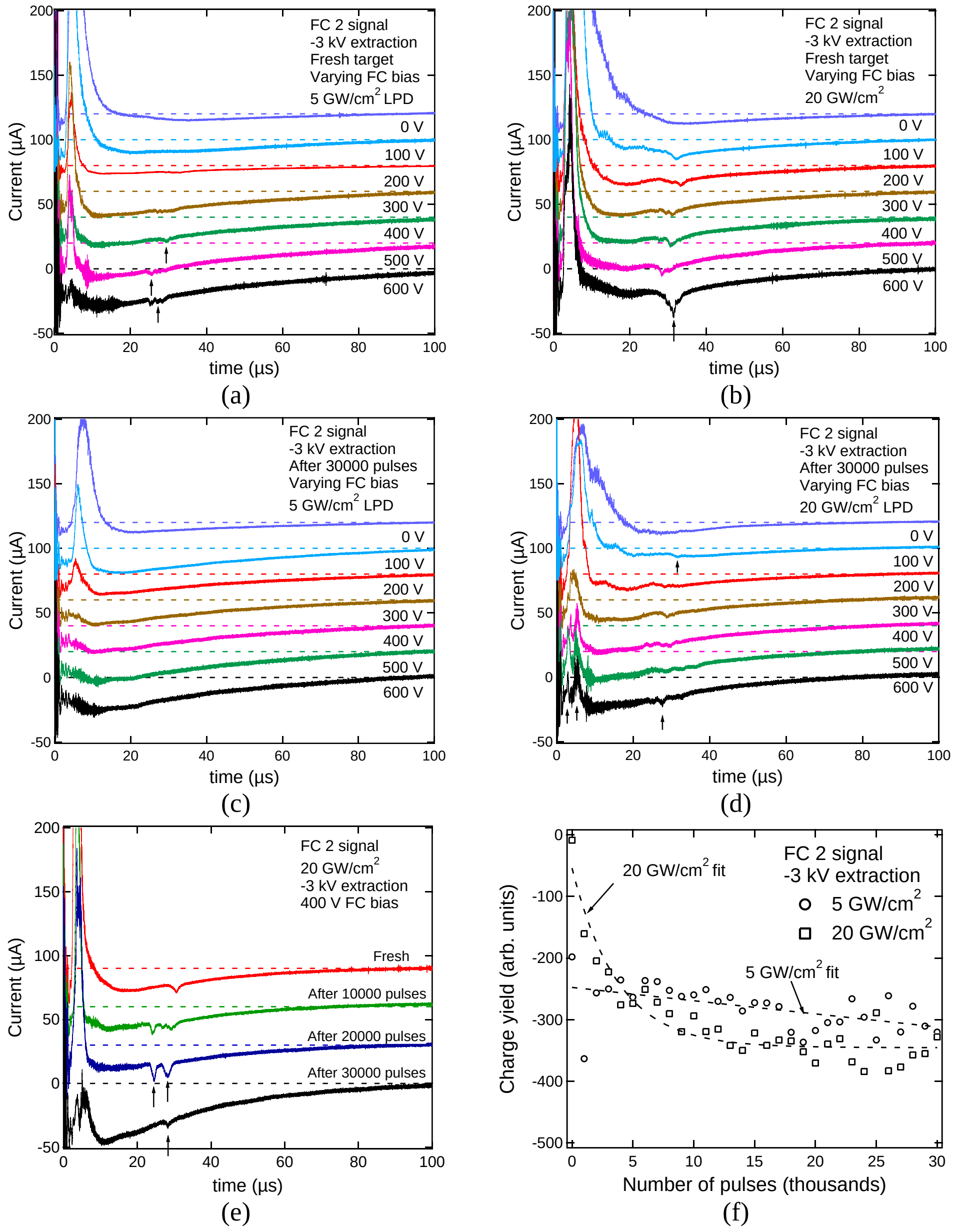

FIGURE 6. FC 2 signal distribution for -3 kV extraction potential for fresh target with varying Faraday cup front plate bias at (a) 5 and (b) 20 GW/cm^2 laser power densities; FC 2 signal distribution for -3 kV extraction potential after 30000 shots with varying Faraday cup front plate bias at (c) 5 and (d) 20 GW/cm^2 laser power densities (e) FC2 signal distributions at 20 GW/cm^2 laser power density at -3 kV extraction and 400 V Faraday cup front plate bias for increasing number of pulses (f) Charge yield for increasing number of pulses obtained from TOF signals at 5 and 20 GW/cm^2 laser power density at -3 kV extraction.

Signals for increasing number of pulses at 20 GW/cm^2 laser power density at -3 kV extraction voltage and 400 V front bias plate retardation voltage are shown in Fig. 6(e). Distinct ion peaks are detected from fresh to 20000 pulses target condition, with a double peak at 24 and 28 μs shown after 20000 shots corresponding to C_{26}^- and C_{35}^- ions respectively. Upon reaching 30000 shots, the negative peak at 28 μs becomes less distinct at -33 μA current, while the 24 μs peak was not detected. In analyzing the change in extracted negative ion yield after the main carbon peak with increasing number of pulses, the charge yield is obtained from the time integration of TOF signals from 20 to 30 μs at -3 kV extraction for up to 30000 pulses for 5 and 20 GW/cm^2 laser power density and 0 V retardation potential, as shown in Fig. 6(f). Increase in negative charge yield is observed for both laser power densities, with an approximately threefold increase observed for 20 GW/cm^2 laser power density, whose rate of negative charge yield increase is higher than that of the 5 GW/cm^2 laser power density.

DISCUSSION

For the case of fresh target ablation, the plasma is initiated at the target surface followed by free expansion along the target surface normal. For ablation directed inside the cavity, a hole of approximately 3 mm depth is formed so the laser is incident at a 12º angle with the hole center, and the plasma is initiated at the surface located at the region of maximum depth. Formation of the plasma within the hole causes the shift in the TOF signal peaks, indicating the reduction in ion flight velocity. In comparing the ion flight velocities for the fresh and ablated target conditions, the velocity difference Δv is calculated from the TOF by:

$$\Delta v = v_{30000} - v_{fresh} \tag{1}$$

where v_{fresh} and v_{30000} represent the ion velocities for the fresh and after 30000 pulses target conditions, respectively. The kinetic energy difference ΔKE is calculated by:

$$\Delta KE = \frac{1}{2} m \left[\left(\frac{d+h}{t_{30000}} \right)^2 - \left(\frac{d}{t_{fresh}} \right)^2 \right] \tag{2}$$

where m is the mass of the C_3^+ ion, d is the flight distance measured from the target surface, h is the ablation depth, t_{30000} and t_{fresh} correspond to the TOF for the post-30000 pulses ablation and fresh target, respectively. From the TOF signals detected by FC 2 for 5 GW/cm^2 laser power density at -3 kV extraction shown in Fig. 5(a), the time difference between the C_3^+ ion peak waveforms for the fresh and after 30000 pulses ablation is 3 μs, which corresponds to a Δv of -45 km/s and a ΔKE of -1.6 keV. As the number of pulses is increased, the formation of a cavity impedes the escape of ions towards the target opening. Ions formed inside the cavity collide with the inner wall and lose kinetic energy thus causing the shift towards later time of arrival towards the FC. The significant decrease in the C_3^+ ion peak may be due to those ions which were unable to travel outside the deep cavity. Positive and negative ions, as well as neutrals which were able to escape the hole propagate in the direction perpendicular to the surface. In describing the flow of the plasma plume vapor within the cavity, it is assumed that this vapor is characterized by a temperature equal to the surface and follows a one-dimensional Maxwellian distribution [13]. The vapor velocity $v_{vap,s}$ at a surface temperature T_s is approximated by:

$$v_{vap,s} = \sqrt{\frac{2kT_S}{\pi m}} \tag{3}$$

where k is the Boltzmann constant. For T_s = 15000 K at 5 GW/cm^2 laser power density, the corresponding vapor velocity and propagation time through the 3 mm hole are 1.4 km/s and 2 μs, respectively [14]. The time it takes for the entire process of nanosecond laser pulse incidence, graphite target vaporization, and subsequent decrease in ablation rate after the pulse is reported to be within 50 ns [14]. Since the decrease of ablation rate can be interpreted as the onset of vapor cooling, the vapor propagation time inside the cavity is sufficient to undergo cooling and further collisions with the wall and among its constituents. In describing the role of the cavity in the formation mechanism of negative ions, we recall that a mechanism for negative ion production in laser plasmas is collision induced electron attachment shown as [7]:

$$A^0 + e^- + e^- \to A^- + e^- \tag{4}$$

With the plasma plume constricted in the cavity, the mean free path of the plume constituents decreases with the propagation volume thus increasing the probability for electron attachment to neutral atoms. The cavity wall contributes to the above mechanism and is suggested to undergo a three body recombination process, as a neutral component M, assuming elastic collisions of electrons with the cavity:

$$A^0 + e^- + e^- + M \to A^- + e^- + M \tag{5}$$

For a vapor temperature T_s = 25000 K at 20 GW/cm^2, the corresponding energy is 2.15 eV, which is less than the 4 eV work function of graphite. This suggests collisions with the cavity wall will not produce additional electrons. The cavity may also contribute to the destruction of negative ions. For the case of the negative peak loss after 30000 pulses in Figs. 6(c) and (d), mechanisms in the destruction of large negative ions (denoted as AB) may involve: (a) electron detachment and (b) dissociative attachment, whose reactions are shown in Eqs. (6) and (7), respectively [7, 15]:

$$AB^- + e^- + M \rightarrow AB^0 + e^- + e^- + M \tag{6}$$

$$AB^- + e^- + M \rightarrow A^- + B^0 + e^- + e^- + M \tag{7}$$

A reaction pathway caused by the cavity enhanced vapor constriction could lead to the further attachment of the smaller neutrals with electrons, which is observed by broadening in Fig. 6(d). In Fig. 6(e), the C_{26}^- and C_{35}^- peaks after 20000 pulses ablation is more distinct than that after 30000 pulses, which suggests that the cavity reaches a depth where the effect of collision induced detachment mechanism leading to negative ion destruction becomes significant. Increase in negative ion production for higher laser power densities may be due to higher ablated neutrals available for attachment, which also increases the probability for subsequent destruction via collision-induced electron attachment due to higher amount of electrons produced. Investigation of the amount of negative ions produced with increasing number of pulses is shown via the charge yield plots in Figs. 4(c) and 6(f). From the charge yield results in Fig. 4(c) for 0 V extraction, the decrease of positive charge yield is observed. On the other hand, increase in the overall extracted negative charge yield at -3 kV extraction in Fig. 6(f) for increasing number of pulses up to 30000 shots is observed, which shows that negative ion production processes dominate over negative ion destruction with increasing cavity depth. Charge yield approaches the same value for increasing number of pulses which may be due to the increase in negative ion destruction for both laser power densities. The rapid increase in negative charge yield for the first 10000 pulses suggests a high rate of negative ion production observed at the onset of cavity development.

SUMMARY

The influence of target cavity formation via repeated nanosecond pulsed laser ablation in the time-of-flight spectra of carbon laser plasmas is investigated. Collected positive and negative signals increase with laser power density. Increase in number of pulses decreases positive signal and increases negative signal during extraction under negative extraction bias. Negative ion peaks are detected by reducing the positive ion beam by means of a potential retardation plate installed in front of the Faraday cup array. Collision-induced processes are suggested in the formation, as well as the destruction of negative ions as the plasma relaxation process within the cavity. Charge yield obtained from the TOF spectra after the C_3^+ ion peak shows increase in negative ion production with increasing number of pulses. Further work will continue to confirm the influence of the cavity in the energy characteristics of the formed negative ions.

REFERENCES

1. S. Vučković, M. Svanqvist, and V. N. Popok, Rev. of Sci. Instr. **79**, 073303 (2008).
2. X. Kong, S. Li, S. Zhang, T. Huang, and Y. Cheng, J. Am. Soc. Mass Spectrom. **22,** 2033-2041 (2011).
3. P. Pradel, P. Monchicourt, J.J. Laucagne, M. Perdrix and G. Watel, Chem. Phys. Letters **158** 412-416 (1989).
4. K. Shibagaki, T. Kawashima, K. Sasaki, and K. Kadota, Jpn. J. Appl. Phys. **39** 4959–4963 (2000).
5. T. Itina, K. Gouriet, L. Zhigilei, and S. Noël, Appl. Surf. Sci. **253**, 7656–7661 (2007).
6. Md. H. A. Shaim and H. E. Elsayed-Ali, J. Appl. Phys. **122**, 203301 (2017).
7. S. S. Alimpiev, M.E. Belov, V.V. Mlinsky, S.M. Nikiforov, V.I. Romanjuk, C. D. Smith, and E. F. Jones, Appl. Phys. A **58**, 67-72 (1994).
8. A. A. Tuinman, A. S. Lahamer, and R. N. Compton, Int. J. Mass. Spec. **205**, 309-323 (2001).
9. T. Moriwaki, H. Shiromaru, Y. Achiba, Z. Phys. D **37**, 169-174 (1996).
10. G. Q. Saquilayan, and M. Wada, AIP Conf. Proc. 1869, 040003 (2017).
11. F. Kokai, Y. Koga, and R.B. Heimann, Appl. Surf. Sci. **96-98** 261-266 (1996).
12. N. A. Vasantgadkar, U. V. Bhandarkar, and S. S. Joshi, Thin Solid Films **519** 1421-1430 (2010).
13. A. Bogaerts, Z. Chen, R. Gijbels, A. Vertes, Spectrochim. Acta B **58** 1867–1893 (2003).
14. S. Sinha, J. Laser Appl. **30**, 012008 (2018).
15. E. Stoffels, W. W. Stoffels, and G. M. W. Kroesen, Plasma Sources Sci. Technol. **10**, 311-317 (2001).